The 9th European Congress on Computational Methods in Applied Sciences and Engineering
ECCOMAS Congress 2024
3–7 June 2024, Lisboa, Portugal

EXPLORING PLASTICITY MATERIAL MODELS IN LEVEL-SET TOPOLOGY OPTIMIZATION

MATTEO POZZI[1,*], ALEXANDRE T. R. GUIBERT[2], H. ALICIA KIM[2] AND FRANCESCO BRAGHIN[1]

[1] Department of Mechanical Engineering
Politecnico di Milano
Via G. La Masa, 1, Milan, 20156, MI, Italy
e-mail: matteo1.pozzi@polimi.it, francesco.braghin@polimi.it

[2] Structural Engineering Department
University of California San Diego
9500 Gilman Dr, La Jolla, 92093, CA, USA
email: aguibert@ucsd.edu, alicia@ucsd.edu

Key words: Plasticity models, level-set topology optimization, COMSOL Multiphysics

Summary. This work investigates various elastoplastic material models in topology optimization. A novel topology optimization framework using the level-set method and COMSOL Multiphysics is proposed to handle the complexities introduced by nonlinear material behaviors. This method broadens the range of applicable plasticity models and streamlines nonlinear analysis in topology optimization.

1 INTRODUCTION

Plasticity material models capture the transition from elastic to plastic behavior, which is crucial for accurately predicting the performance of materials under various loading conditions. Integrating these models into structural optimization allows engineers to design structures that are both material-efficient and resilient to mechanical loading. This is particularly important in industries such as aerospace, automotive, and civil engineering, where safety, durability, and cost-effectiveness are fundamental.

Consequently, plasticity material models have garnered significant attention in structural optimization, providing a robust framework to design resilient structures capable of withstanding mechanical loads while minimizing material usage. For instance, [1] employed an elastoplastic von Mises material model with linear isotropic hardening to maximize structural ductility under volume constraints, using the Solid Isotropic Material with Penalization (SIMP) approach but limited to 2D examples. Similarly, [2] explored plastic work objectives using a fine strain plasticity model. [3] aimed to prevent plastic strains through stress-constrained topology optimization, while [4] emphasized adjoint sensitivity analysis with anisotropic plastic models. [5, 6, 7] extended the framework to finite strain viscoplastic systems and periodic micro-structures, highlighting the challenges of numerical stability and the importance of initial conditions. [8] introduced a level-set method for shape optimization under quasi-static plasticity, demonstrating its application in both 2D and 3D examples. The works of [9, 10, 11] explored alternative methods such as Evolutionary Structural Optimization (ESO), Bi-directional Evolutionary Structural

Optimization (BESO), and Second Order Cone Programming (SOCP), respectively, each contributing unique approaches to handle stress constraints, compliance minimization, and volume reduction. Despite the advancements, most studies remain limited to 2D examples and utilize the von Mises plasticity model, indicating the need for further exploration into more complex plasticity models and 3D problem settings.

One of the main challenges lies in the nonlinear finite element analysis which, in the case of plasticity, leads to path-dependent solutions [12]. Consequently, the associated sensitivity analysis also becomes path-dependent, thus requiring an incremental (explicit scheme) procedure [13, 1]. Moreover, different plasticity models might require different implementations and solution algorithms [12]. These inherent challenges impose significant constraints on the integration of diverse plasticity models into topology optimization algorithms. For this reason, a limited number of studies address material nonlinearities, and the majority of them focus on von Mises plasticity with linear isotropic hardening.

For this reason, a flexible topology optimization framework called ParaLeSTO-COMSOL [14] is developed to handle different plasticity models with little to no changes to the code implementation. In this framework, automatic differentiation techniques are leveraged to streamline sensitivity analysis and facilitate the exploration of diverse plasticity parameters.

2 ELASTOPLASTIC MATERIAL MODELS

Plastic material models are used in engineering to describe the behavior of materials under plastic deformation, where they undergo permanent changes in shape or size when subjected to stress [12]. Usually, a yield criterion is used to define the stress condition under which plastic deformation occurs. Stress paths inside the yield surface result in purely recoverable deformations (elastic behavior), while paths intersecting the yield surface produces both recoverable and permanent deformations (plastic strains). In this work, we focus on the metal plasticity under the von Mises criterion [12], whose yield surface F_y takes the form of

$$F_y = \sigma_e - \sigma_y \leq 0 \tag{1}$$

$$\sigma_e = \sqrt{\frac{3}{2}\mathrm{dev}(\boldsymbol{\sigma}) : \mathrm{dev}(\boldsymbol{\sigma})} \tag{2}$$

$$\dot{\varepsilon}_{pe} = \sqrt{\frac{3}{2}\mathrm{dev}(\dot{\boldsymbol{\varepsilon}}_p) : \mathrm{dev}(\dot{\boldsymbol{\varepsilon}}_p)} \tag{3}$$

where σ_e is the effective or von Mises stress, σ_y is the yield stress, $\dot{\varepsilon}_{pe}$ is the effective plastic strain rate, $\mathrm{dev}(\cdot)$ is the deviatoric operator, $\boldsymbol{\sigma}$ is the stress tensor, and $\dot{\boldsymbol{\varepsilon}}_p$ is the plastic strain tensor increment.

The plastic strain tensor increment is computed using the associated flow rule [12]:

$$\dot{\boldsymbol{\varepsilon}}_p = \lambda \frac{\partial \sigma_e}{\partial \boldsymbol{\sigma}} \tag{4}$$

where λ is the plastic multiplier such that $\lambda \geq 0$ and $\lambda F_y = 0$.

The yield stress σ_y [12] is defined as

$$\sigma_y = \sigma_{y,0} + \sigma_h \tag{5}$$

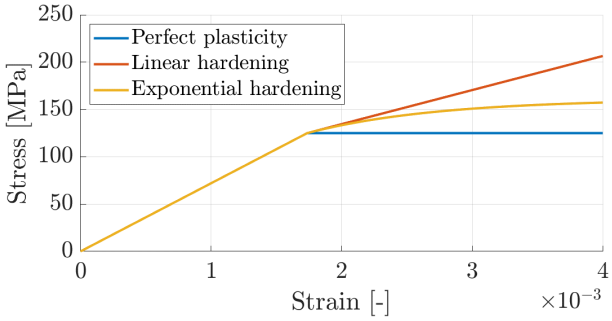

Figure 1: Example of different plastic behaviors.

where $\sigma_{y,0}$ is the initial yield stress, and σ_h is the hardening function that depends on the effective plastic strain ε_{pe}. In case of perfect plasticity, the yield stress remains constant ($\sigma_h = 0$). Otherwise, the hardening function is defined according to the particular isotropic hardening law (Fig 1). For instance, the linear isotropic hardening function [12] is defined as

$$\sigma_h(\varepsilon_{pe}) = H\varepsilon_{pe} \tag{6}$$

where H is the hardening modulus that regulates the slope of the stress-strain curve after the yield point.

For elastoplastic materials, we define the total elastic strain energy [12] of the system as:

$$W_s = \int_\Omega \int_0^T \boldsymbol{\sigma} : \dot{\boldsymbol{\varepsilon}} dt\Omega \tag{7}$$

In the same way, the expression for the plastic dissipation energy [12] is:

$$W_p = \int_\Omega \int_0^T \boldsymbol{\sigma} : \dot{\boldsymbol{\varepsilon}}_p dt\Omega \tag{8}$$

3 LEVEL-SET TOPOLOGY OPTIMIZATION

The optimization problem aims at maximizing the total strain energy W_s of the system subject to a prescribed displacement

$$\begin{aligned} \max_\Omega \quad & W_s \\ \text{s.t.} \quad & \boldsymbol{R}(\boldsymbol{u}) = \boldsymbol{0} \\ & V \leq V_{\max} \end{aligned} \tag{9}$$

where V represents the volume of the structure, $V_{\max}$ is the maximum volume, and $\boldsymbol{R}$ is the nonlinear state equation. In this work, a maximum volume fraction of 30% is used.

Problem (9) is solved iteratively using a level-set topology optimization algorithm [15, 16]. The material properties of the structure are interpolated using the ersatz material interpolation with a linear interpolation scheme [16, 17]. Using the level-set method [18], the structure under optimization, denoted by Ω, is defined as the zero-level of an implicit function $\Phi(x)$:

$$\begin{cases} \Phi(x) \geq 0, & x \in \Omega \\ \Phi(x) = 0, & x \in \partial\Omega \\ \Phi(x) < 0, & x \notin \Omega \end{cases} \tag{10}$$

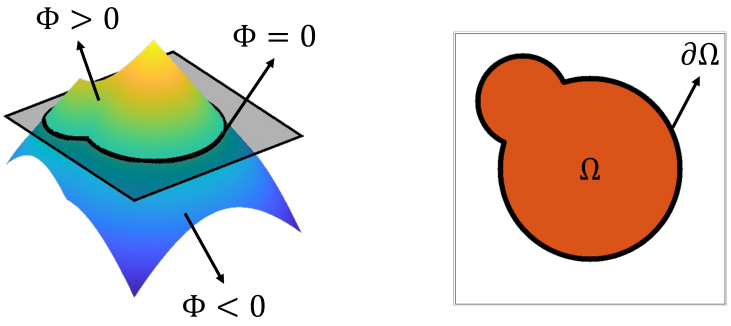

Figure 2: Implicit representation of a two-dimensional shape (right) using a level-set function (left).

At each iteration, the boundary $\partial\Omega$ is updated using the level-set equation [18]:

$$\frac{\partial\Phi(x)}{\partial t} + |\nabla\Phi(x)|V_n(x) = 0 \tag{11}$$

where t denotes pseudo-time, and V_n represents the normal velocity field obtained solving the sub-optimization problem [15, 16].

At each iteration, the sub-optimization problem is defined using the sensitivities of the cost function and the constraints [15, 16]. The sensitivity of a generic function J with respect to a boundary point i is defined through the discrete adjoint method [19]:

$$\frac{dJ}{d\Omega_i} = \sum_{j=1}^{N_e} \frac{\partial J}{\partial \rho_j}\frac{\partial \rho_j}{\partial \Omega_i} \tag{12}$$

where N_e is the number of finite elements used in the discretization grid and ρ_j is the density of element j. The partial derivatives $\partial J/\partial\rho_j$ are evaluated using the reverse mode automatic differentiation method embedded in COMSOL, as explained on the Optimization Module User's Guide.

The complete optimization loop (Fig. 3) is implemented using the open-source code ParaLeSTO-COMSOL. More details regarding the code can be found in [20, 14].

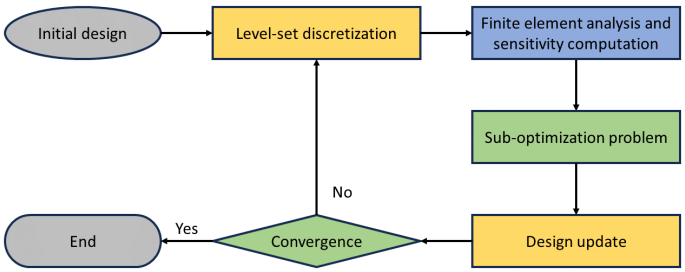

Figure 3: Level-set topology optimization loop [20]. The finite element analysis and the sensitivity computation (blue) are executed using COMSOL. The level-set operations (yellow) and the optimization steps (green) are carried out in MATLAB.

4 NUMERICAL EXAMPLES

The numerical examples are used to investigate the effects of different plasticity parameters and models on the optimal layout. The problem settings and the initial conditions are shown in Fig. 4. The prescribed displacement is applied downward on the green regions, whereas the red regions represent the clamped boundary conditions.

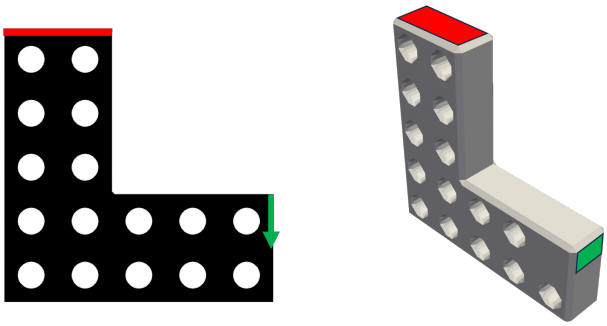

Figure 4: Problem settings and initial conditions for the 2d (left) and 3d (right) numerical examples. The clamp is indicated by the red region, whereas the prescribed displacement is applied downward on the green part.

If not otherwise specified, the material properties are listed in Tab. 1.

	Value	Unit
Young's modulus	72	GPa
Poisson's coefficients	0.3	-
Initial yield stress	125	MPa
Isotropic hardening modulus	573	MPa

Table 1: Default material properties used in the examples.

4.1 2D L-beam problem

The first numerical example is a 2-dimensional L-beam structure. The design domain ($1.0\,\mathrm{m} \times 1.0\,\mathrm{m}$) is discretized using a 100×100 structured grid with linear square elements. The plane strain approximation is used, with a thickness of $0.01\,\mathrm{m}$. The problem settings are shown in Fig. 4.

The optimization problem (9) is solved first using the linear elastic material model, and then using the von Mises plasticity with linear isotropic hardening (Eq. (6)). The optimal results are shown in Fig. 5.

The performances of both structures are then evaluated using the plastic material model to obtain the von Mises stress distribution (Fig. 6).

The layout optimized using the plasticity model has a less stress variation compared to the one optimized for elasticity. This results in a 38.5% higher strain energy and in a 13.6% lower plastic dissipation (Tab. 2). On the other hand, the structure optimized for elasticity performs

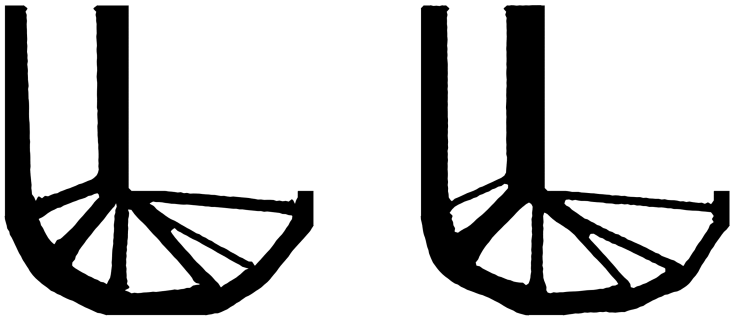

Figure 5: Optimal layouts obtained from Fig. 4 using linear elasticity (left) and von Mises plasticity with linear isotropic hardening (right).

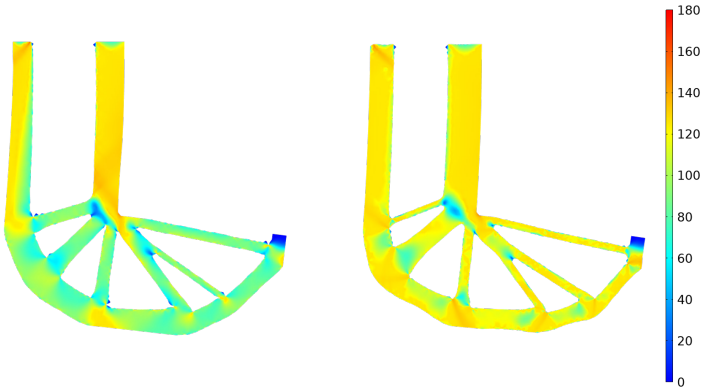

Figure 6: Evaluation using the plastic material model of the structures in Fig. 5. The figures show the von Mises stress distribution (MPa).

better than the plasticity one when we evaluate them using the linear elastic material (Tab. 2), with a 4.5% higher strain energy.

	Elastic optimization	Plastic optimization
Elastic response	$W_s = 0.92\,\text{kJ}$	$W_s = 0.88\,\text{kJ}$
Plastic response	$W_s = 0.26\,\text{kJ}$ $W_p = 0.44\,\text{kJ}$	$W_s = 0.36\,\text{kJ}$ $W_p = 0.38\,\text{kJ}$

Table 2: Strain energy cross validation of the optimal layouts in Fig. 5.

4.2 3D L-beam problem

In the second example, we consider the 3-dimensional L-beam structure shown in Fig. 4. The design domain ($1.0\,\text{m} \times 1.0\,\text{m} \times 0.2\,\text{m}$) is discretized using a $50 \times 50 \times 10$ structured grid made of linear cube elements. A prescribed vertical displacement of $0.02\,\text{m}$ is used. Starting from the structure in Fig. 4, the optimization problem (9) is solved using the elasticity model and the von Mises plasticity with linear isotropic hardening.

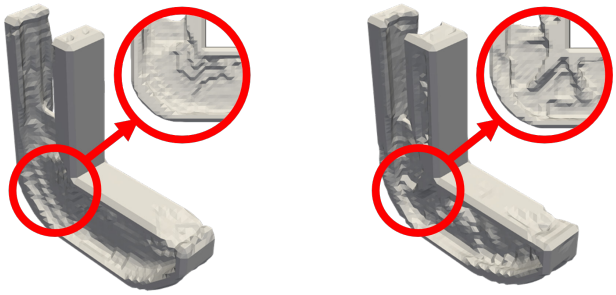

Figure 7: Optimal layouts obtained from Fig. 4 using the linear elasticity (left) and the von Mises plasticity with linear isotropic hardening (right).

The main geometric differences between the two optimal results (Fig. 7) are the supporting features that appear in the region of the corner. To evaluate the effect of these features, the two structures are evaluated using the plasticity material model with different prescribed displacements. In this way, the loading curves of strain energy, plastic dissipation, and reaction force are reconstructed. In the elastic region (green background), the responses of the two structures are similar. On the other hand, as the material enters the plastic region (red background), the two responses become different. In particular, at the maximum displacement, the strain energy is 23.3% higher, the plastic dissipation is 11.5% lower, and the reaction force is 18.2% higher.

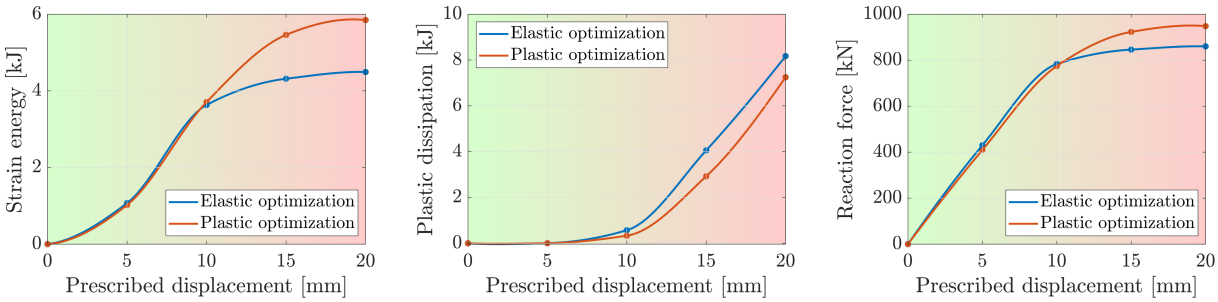

Figure 8: Loading curves of the structures in Fig. 7. The strain energy, the plastic dissipation, and the reaction force are evaluated. The material behavior changes from mostly elastic (green background) to mostly plastic (red background) as the prescribed displacement increases.

4.3 Effect of the hardening modulus

In the third example, we examine how the optimal result varies with different values of the linear hardening modulus. This modulus controls the slope of the stress-strain curve after the yielding point.

The same problem settings of Sec. 4.2 are used. Problem (9) is solved using different values of H, and Fig. 9 shows the optimal results obtained with $H = 720\,\text{MPa}$ and $H = 36000\,\text{MPa}$. From Fig. 9 we observe that a higher hardening modulus results in thinner supporting features. This is because materials with higher hardening modulus can withstand greater stress before

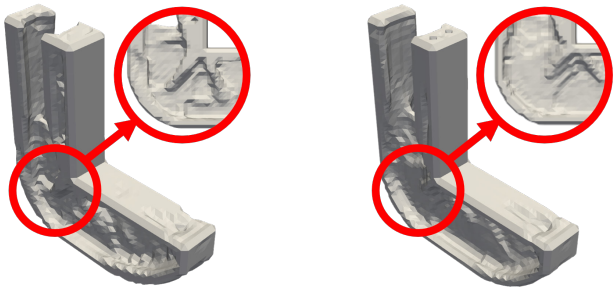

Figure 9: Optimal layouts obtained with $H = 720\,\text{MPa}$ (left) and $H = 36000\,\text{MPa}$ (right).

undergoing significant plastic deformation.

4.4 Effect of the initial yield stress

The fourth example is used to investigate how the optimal result changes when using different values for the initial yield stress $\sigma_{y,0}$. This parameter controls the size of the elastic region of the material.

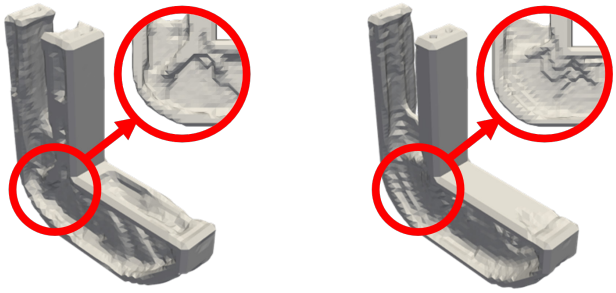

Figure 10: Optimal layouts obtained with $\sigma_{y,0} = 100\,\text{MPa}$ (left) and $\sigma_{y,0} = 250\,\text{MPa}$ (right).

The same problem settings of Sec. 4.2 are used. The optimal results obtained with $\sigma_{y,0} = 100\,\text{MPa}$ and $\sigma_{y,0} = 250\,\text{MPa}$ are shown in Fig. 10. As the initial yield stress of the material increases, the supporting features disappear, and the elastoplastic solution tends to the elastic solution. Higher initial yield stress indicates that the material can endure higher loads before yielding, thus reducing the necessity for elastoplastic considerations in design.

4.5 Linear vs. exponential isotropic hardening

With the last example, we compare the results obtained using the linear (Eq. (6)) and the exponential (Eq. (13)) isotropic hardening models. The exponential hardening function is defined using the Voce model [12]:

$$\sigma_h(\varepsilon_{pe}) = \sigma_{\text{sat}}(1 - e^{-\beta\varepsilon_{pe}}) \tag{13}$$

where $\beta = 10^3$ and σ_{sat} is equal to H/β in order for the two hardening functions in Fig. 11 to have the same slope at the yield point ($\varepsilon_{ep} = 0$). In this example, the parameters $H = 36000\,\text{MPa}$ and $\sigma_{y,0} = 125\,\text{MPa}$ are used.

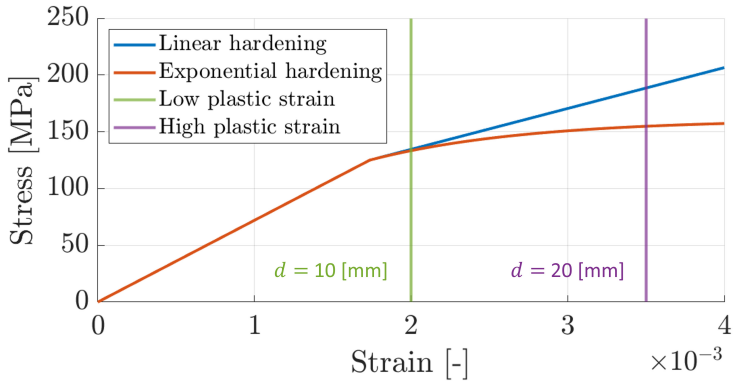

Figure 11: Linear and exponential hardening functions.

The optimization is performed using two different prescribed displacements (Fig. 11). The first one ($d = 0.01\,\text{m}$) generates small plastic strains for which the two hardening curves have similar values. On the other hand, the second displacement ($d = 0.02\,\text{m}$) produces larger plastic strains for which the difference between the two curves are more substantial. The optimal results are collected in Tab. 3, while Fig. 12 shows the optimal layout obtained using the greater displacement.

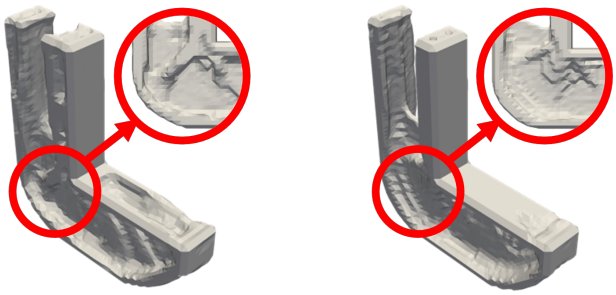

Figure 12: Optimal layouts obtained using the linear (left) and the exponential (right) isotropic hardening curves.

The results obtained using small displacements are similar, as shown in the first row of Tab. 3. This similarity arises because small displacements induce minor plastic strains, making the two hardening functions comparable. In contrast, the large displacements lead to significant plastic strains, highlighting the differences between the hardening functions. Therefore, the difference in the optimal result is more significant in the second row of Tab. 3.

The magnitude of the hardening function, which describes how the material's resistance to plastic deformation increases, is more relevant than its specific shape. This implies that the

	Linear hardening	Exponential hardening
Small displacement ($d = 0.01\,\mathrm{m}$)	$W_s = 3.94\,\mathrm{kJ}$ $W_p = 0.43\,\mathrm{kJ}$	$W_s = 3.90\,\mathrm{kJ}$ $W_p = 0.37\,\mathrm{kJ}$
Large displacement ($d = 0.02\,\mathrm{m}$)	$W_s = 9.02\,\mathrm{kJ}$ $W_p = 6.43\,\mathrm{kJ}$	$W_s = 7.78\,\mathrm{kJ}$ $W_p = 6.86\,\mathrm{kJ}$

Table 3: Optimal results obtained using the linear and the exponential hardening curves with two prescribed displacements. The values of the optimal strain energy W_s and plastic dissipation W_p are show.

overall ability of the material to harden under stress is more critical in determining structural performance than the detailed characteristics of how this hardening occurs.

5 CONCLUSIONS

The performance evaluation of topologically optimized structures for elastoplasticity reveals that purely elastic solutions exhibit suboptimal performance when assessed against elastoplastic models. A significant advantage of elastoplastic solutions is their ability to incorporate supporting features that mitigate plastic strains, enhancing the robustness and resilience of the design.

The developed ParaLeSTO-COMSOL framework effectively handles various plasticity models with minimal implementation changes. Using this framework, key parameters influencing the optimal layouts, such as hardening modulus, initial yield stress, and the magnitude of the hardening function, have been investigated.

Future research should focus on developing advanced materials with tailored properties and examining the effects of dynamic conditions and temperature variations. This approach will provide a more comprehensive understanding of material behavior in the context of topology optimization.

ACKNOWLEDGMENTS

The support of the H2020 FET-proactive Metamaterial Enabled Vibration Energy Harvesting (MetaVEH) project under Grant Agreement No. 952039 is acknowledged.

References

[1] S. Schwarz, K. Maute, E. Ramm, Topology and shape optimization for elastoplastic structural response. Computer Methods in Applied Mechanics and Engineering **190**, 2135–2155 (2001). https://doi.org/10.1016/S0045-7825(00)00227-9

[2] M. Wallin, V. Jönsson, E. Wingren, Topology optimization based on finite strain plasticity. Structural and Multidisciplinary Optimization **54**, 783–793 (2016). https://doi.org/10.1007/s00158-016-1435-0

[3] O. Amir, Stress-constrained continuum topology optimization: a new approach based on elasto-plasticity. Structural and Multidisciplinary Optimization **55**, 1797–1818 (2017). https://doi.org/10.1007/s00158-016-1618-8

[4] G. Zhang, L. Li, K. Khandelwal, Topology optimization of structures with anisotropic plastic materials using enhanced assumed strain elements. Structural and Multidisciplinary Optimization **55**, 1965–1988 (2017). https://doi.org/10.1007/s00158-016-1612-1

[5] N. Ivarsson, M. Wallin, D. Tortorelli, Topology optimization of finite strain viscoplastic systems under transient loads. International Journal for Numerical Methods in Engineering **114**, 1351–1367 (2018). https://doi.org/10.1002/nme.5789

[6] N. Ivarsson, M. Wallin, D.A. Tortorelli, Topology optimization for designing periodic microstructures based on finite strain viscoplasticity. Structural and Multidisciplinary Optimization **61**, 2501–2521 (2020). https://doi.org/10.1007/s00158-020-02555-x

[7] N. Ivarsson, M. Wallin, O. Amir, D.A. Tortorelli, Plastic work constrained elastoplastic topology optimization. International Journal for Numerical Methods in Engineering **122**, 4354–4377 (2021). https://doi.org/10.1002/nme.6706

[8] J. Desai, G. Allaire, F. Jouve, C. Mang, Topology optimization in quasi-static plasticity with hardening using a level-set method. Structural and Multidisciplinary Optimization **64**, 3163–3191 (2021). https://doi.org/10.1007/s00158-021-03034-7

[9] B. Blachowski, P. Tauzowski, J. Lógó, Yield limited optimal topology design of elastoplastic structures. Structural and Multidisciplinary Optimization **61**, 1953–1976 (2020). https://doi.org/10.1007/s00158-019-02447-9

[10] Y. Han, B. Xu, Q. Wang, Y. Liu, Z. Duan, Topology optimization of material nonlinear continuum structures under stress constraints. Computer Methods in Applied Mechanics and Engineering **378**, 113731 (2021). https://doi.org/10.1016/j.cma.2021.113731

[11] X. Zhang, X. Li, Y. Zhang, A framework for plasticity-based topology optimization of continuum structures. International Journal for Numerical Methods in Engineering **124**, 1493–1509 (2023). https://doi.org/10.1002/nme.7172

[12] N.S. Ottosen, M. Ristinmaa, in *The Mechanics of Constitutive Modeling*, ed. by N.S. Ottosen, M. Ristinmaa (Elsevier Science Ltd, Oxford, 2005), pp. 203–246. https://doi.org/10.1016/B978-008044606-6/50009-6

[13] K. Maute, S. Schwarz, E. Ramm, Adaptive topology optimization of elastoplastic structures. Structural Optimization **15**, 81–91 (1998). https://doi.org/10.1007/BF01278493

[14] A.T. Guibert, J. Hyun, A. Neofytou, H.A. Kim, *Implementation of a Plug-and-Play Reusable Level-Set Topology Optimization Framework via COMSOL Multiphysics*, in *American Institute of Aeronautics and Astronautics* (2023), p. 1675. https://doi.org/10.2514/6.2023-1675

[15] M.Y. Wang, X. Wang, D. Guo, A level set method for structural topology optimization. Computer Methods in Applied Mechanics and Engineering **192**, 227–246 (2003). https://doi.org/10.1016/S0045-7825(02)00559-5

[16] G. Allaire, F. Jouve, A.M. Toader, Structural optimization using sensitivity analysis and a level-set method. Journal of Computational Physics **194**, 363–393 (2004). https://doi.org/10.1016/j.jcp.2003.09.032

[17] M. Dambrine, D. Kateb, On the ersatz material approximation in level-set methods. ESAIM: Control, Optimisation and Calculus of Variations **16**, 618–634 (2010). https://doi.org/10.1051/cocv/2009023

[18] S. Osher, R. Fedkiw, *Level Set Methods and Dynamic Implicit Surfaces*, vol. 153 (Springer New York, 2003). https://doi.org/10.1007/b98879

[19] S. Kambampati, H. Chung, H.A. Kim, A discrete adjoint based level set topology optimization method for stress constraints. Computer Methods in Applied Mechanics and Engineering **377**, 113563 (2021). https://doi.org/10.1016/j.cma.2020.113563

[20] C.M. Jauregui, J. Hyun, A. Neofytou, J.S. Gray, H.A. Kim, Avoiding reinventing the wheel: reusable open-source topology optimization software. Structural and Multidisciplinary Optimization **66**, 145 (2023). https://doi.org/10.1007/s00158-023-03589-7